CHEMISTRY OF MATERIALS
Article

Chem. Mater. **2010,** *22,* 6153–6161 6153
DOI:10.1021/cm102134k

Gadolinium−Europium Carbonate Particles: Controlled Precipitation for Luminescent Biolabeling

Séverine Lechevallier,*,† Pierre Lecante,† Robert Mauricot,† Hervé Dexpert,† Jeannette Dexpert-Ghys,† Hoi-Kuan Kong,‡ Ga-Lai Law,§ and Ka-Leung Wong‡

†*Centre d'Elaboration de Matériaux et d'Etudes Structurales, 29 rue Jeanne Marvig, BP 94347, 31055 Toulouse Cedex 4, France,* ‡*Department of Chemistry, Hong Kong Baptist University, Kowloon Tong, Hong Kong, and* §*Department of Chemistry, The University of Hong Kong, Pokfulam, Hong Kong*

Received July 30, 2010. Revised Manuscript Received September 17, 2010

Europium-doped gadolinium carbonates particles have been prepared via urea-assisted precipitation. The reaction has been followed step by step with the investigations of the precipitate by transmission electron microscopy and wide-angle X-ray scattering, in relation with infrared absorption and thermal analyses. It has been observed that spherical particles of $(Gd_{0.95}Eu_{0.05})(OH)CO_3$, monodispersed in size and amorphous, precipitate first and then transform to agglomerated platelike crystals of $(Gd_{0.95}Eu_{0.05})_2(CO_3)_3 \cdot 2H_2O$ as the precipitation continues. The Eu^{3+} $^5D_0 \rightarrow {}^7F_J$ emission spectrum and the $^5D_0$ lifetime in the two carbonate matrices have been measured. Selected hydroxycarbonate nanoparticles (NPs), with diameters of 164 ± 20 nm, have been then transformed to oxide NPs having the cubic crystalline structure C-$(Gd_{0.95}Eu_{0.05})_2O_3$, with the same shape and size. The photoluminescence (PL) properties of hydroxycarbonate and oxide NPs, and of their colloidal suspensions in water, have been investigated. The hydroxycarbonate and the oxide NPs exhibit same PL intensities when excitation is achieved in one of the $Eu^{3+}(4f^6)$ levels. Tests of in vitro fluorescence imaging have been performed. The luminescent NPs have been observed after their internalization by human cervical carcinoma (HeLa) cells. It is concluded that the controlled (urea-assisted) precipitation is appropriate to synthesize $Gd(OH)CO_3$:Eu^{3+} and Gd_2O_3:Eu^{3+} nanoparticles having adequate characteristics for biolabeling.

1. Introduction

Gadolinium and yttrium sesquioxides crystallize in the same cubic phase; this phase is usually called C-Ln_2O_3 ($Ia\bar{3}$ space group). The emission and excitation spectra of Eu^{3+} partially substituting the Ln^{3+} (Ln = Gd or Y) in these hosts have been thoroughly investigated in refs 1−7, among many other literature. The $(Y_{1-x}Eu_x)O_{1.5}$ compound, with $x \approx 0.05$ (which is more usually denoted as Y_2O_3:Eu^{3+}), is one of the most largely used red phosphors in lighting or emissive displays. Recently, the search for nanoparticles NPs with controlled properties has renewed the interest for these compounds. In the field of luminescent labeling, the possible use of europium oxide nanoparticles in an immunoassay for atrazine has been demonstrated by Feng et al.,[8] and several applications related to optical detection of antibodies by Gd_2O_3:Eu^{3+} nanoparticles have then been shown by the same group of scientists.[9,10] More recently, nanoparticles that have both luminescent (Gd_2O_3:Eu^{3+}) and magnetic (Fe_2O_3:Nd^{3+},Co^{2+}) components have been employed in multiplexed immunoassays.[11] Bridot et al.[12] have also demonstrated that Gd_2O_3 nanoparticles may be used as contrast agents in MRI (magnetic resonance imaging), whereas a coating of organic dye on these nanoparticles brings the luminescence function. The same group has engineered hybrid nanoparticles with the possibility to follow the long-term luminescence of the core Gd_2O_3:Tb^{3+} and the short-term luminescence of the organic coating.[13] On the other hand, bimodal (fluorescence + magnetic) imaging of cancer cells by Y_2O_3:Eu^{3+},Gd^{3+} nanocrystals has been demonstrated in ref 14.

*Author to whom correspondence should be addressed. Tel.: +(33)5 62 25 78 47. Fax: +(33)5 62 25 79 99. E-mail: severine.lechevallier@cemes.fr.

(1) Chang, N. C.; Gruber, J. B *J. Chem. Phys.* **1964**, *41*, 3227.
(2) Heber, J.; Hellwege, K. H.; Köbler, U.; Murmann, H. *Z. Phys.* **1970**, *237*, 189.
(3) Dexpert-Ghys, J.; Faucher, M. *Phys. Rev. B* **1979**, *20*, 10.
(4) Leavitt, R. P.; Gruber, J. B.; Chang, N. C.; Morrison, C. A. *J. Chem. Phys.* **1982**, *76*, 4775.
(5) Hunt, R. B.; Pappalardo, R. G. *J. Lumin.* **1985**, *34*, 133.
(6) Buijs, M.; Meyerink, A.; Blasse, G. *J. Lumin.* **1987**, *37*, 9.
(7) Tanner, P.; Wong, K.-L. *J. Phys. Chem. B* **2004**, *108*, 136.
(8) Feng, J.; Shan, G.; Maquieira, A.; Koivunen, M. E.; Guo, B.; Hammock, B. D.; Kennedy, I. M. *Anal. Chem.* **2003**, *75*, 5287–.
(9) Nichkova, M.; Dosev, D.; Gee, S. J.; Hammock, B. D.; Kennedy, I. M. *Anal. Chem.* **2005**, *77*, 6864.
(10) Nichkova, M.; Dosev, D.; Perron, R.; Gee, S. J.; Hammock, B. D.; Kennedy, I. M. *Anal. Bioanal. Chem.* **2006**, *384*, 631.
(11) Dosev, D.; Nichkova, M.; Dumas, R. K.; Gee, S. J.; Hammock, B. L.; Kennedy, I. M. Nanotechnology, **2007**, *18*, No. 055102 (6 pp).
(12) Bridot, J. L.; Dayde, D.; Rivière, C.; Mandon, C.; Billotey, C.; Lerondel, S.; Sabattier, R.; Cartron, G.; Blondiaux, G.; Janier, M.; Perriat, P.; Roux, S.; Tillement, O. *J. Am. Chem. Soc.* **2007**, *129*, 5076.
(13) Louis, C.; Bazzi, R.; Marquette, C. A.; Bridot, J. L.; Roux, S.; Ledoux, G.; Mercier, B.; Blum, L.; Perriat, P.; Tillement, O. Chem. Mater. **2005**, *17*, 1673.
(14) Setua, S.; Menon, D.; Asok, A.; Nair, S.; Koyakutty, M. *Biomaterials* **2010**, *31*, 714.

Published on Web 10/25/2010

These studies used various preparation procedures. As a matter of fact, there are many ways to synthesize Ln_2O_3 nanocrystals (with Ln = La−Lu and Y), from temperature vapor-phase reactions[15−18] to several softer routes in solution. Alternatively, the precipitation and decomposition from an aqueous solution of Ln^{3+} salts at moderate temperature (600−700 °C) by spray pyrolysis has been effectively developed by different research groups.[19,20] The generated particles are spherical, submicrometer in size, and made of an amorphous oxide, so that thermal annealing is necessary to achieve the good luminescence properties. Nanoscale particles (< 5 nm) have been directly precipitated with the polyol-mediated method.[21] The precipitation of a Ln^{3+} salt from a water solution, and then its decomposition to Ln_2O_3 by thermal annealing, is, in fact, a more general way to proceed, which avoids the use of organic solvents, because, in contrast, it is necessary in the sol−gel processing of metal alkoxides.

The precipitation, under hydrothermal conditions, of the rare-earth hydroxide at basic pH is one of the routes followed by other researchers.[22−25] The shape and size of the obtained hydroxide particles clearly are strongly dependent on the synthesis conditions. In ref 22, cubic-shaped nanocrystals (10−45 nm) of Y_2O_3:Er^{3+} have been obtained after annealing of the corresponding $Ln(OH)_3$. More often, hydrothermal precipitation yields to the formation of nanorods,[23] or nanotubes.[24,25] The precipitation of rare-earth carbonates has also been considered. Urea appears as a source of carbonate ions, which is specifically advantageous if one wants to synthesize very well-defined monodispersed spherical particles. Phosphors with the formulation M_2O_3:Ln^{3+} (with M = Y, Gd, or Lu and Ln = Eu, Er, Yb, Sm, or Ce) have been synthesized following this procedure, in view of different technological developments.[26−30] At the origin of these investigations is the important work done by Matijevic et al. on the preparation of uniformly sized colloids of a large variety of metal oxides precursors, including those of lanthanides.[31−33]

Table 1. pH of the Reacting Medium, and Size and Shape of the Particles Extracted at Different Reaction Times

name	reaction time (min)	pH	size (nm)	shape
t6	120	6.0	164 ± 22	spherical
t10	180	6.2	230 ± 23	spherical
t12	240	6.2	260 ± 19	spherical
t13	270	6.3	257 ± 39	spherical (+ platelike)
t14	300	6.6	221 ± 39	spherical + platelike
t16	420	7.7		platelets

In this paper, we employed the Matijevic's synthesis as a route to obtain europium-doped gadolinium nanoparticles suitable for use as luminescent labels. A dynamical study at the different steps of the particles formation, based on wide-angle X-ray scattering (WAXS) and Fourier transform infrared (FTIR) analyses, has been undertaken to follow the chemical changes during the maturation of the colloidal suspension. These changes are associated with noticeable modifications in the shape and size of the particles, as evidenced by transmission electron microscopy (TEM) imaging. The photoluminescence (PL) properties of the carbonate nanoparticles extracted at selected reaction times, and then after their thermal treatment to give the oxide, are detailed. The photoluminescence of colloidal suspensions of the particles is also analyzed, and the possibility to employ these NPs for the luminescent imaging of living cells is tested, along the lines already developed by some of us in ref 23.

2. Experimental Section

2.a. Synthesis of the Nanoparticles (NPs). Europium and gadolinium nitrates (99.99%) were stock solutions from Rhodia. Urea (98%) was purchased from Sigma Aldrich.

Europium-doped gadolinium carbonates were synthesized from nitrate precursors in water, following the procedure described by Matijevic and Hsu,[31] based on urea decomposition at temperatures above 60 °C. The optimum concentrations determined in their work were employed here: 5.6×10^{-3} M for gadolinium and europium precursors (0.95Gd/0.05Eu) and 0.5 M for urea. Gadolinium and europium nitrates and urea were dissolved in distilled water, and the solution was placed in a round-bottom flask tightly closed for aging at 85 °C in an oil bath. As the reaction proceeds, changes are observable in the reacting medium. At given reaction times, 25 mL of solution were sampled and centrifuged. The supernatant solution was discarded, and the solid phase was resuspended in water using an ultrasonic bath. The washing procedure was repeated three times, and the washed samples were dried in an oven overnight. The solid phase was then recovered and subjeted to several characterizations with the techniques listed hereafter. Solid samples will be labeled in the following with the notation given in Table 1: from t6, extracted at 120 min, to t16 extracted at 420 min.

(15) Bihari, B.; Eilers, H.; Tissue, B. M. *J. Lumin.* **1997**, *75*, 1.
(16) Gordon, W. O.; Carter, J. A.; Tissue, B. M. *J. Lumin.* **2004**, *108*, 339.
(17) Nicolas, D.; Masenelli, B.; Mélinon, P.; Bernstein, E.; Dujardin, C.; Ledoux, G.; Esnouf, C. *J. Chem. Phys.* **2006**, *125*, No. 171104 (4 pp) .
(18) Dosev, D.; Guo, B.; Kennedy, I. M. *Aerosol Sci.* **2006**, *37*, 402.
(19) Kang, Y. C.; Park, S. B.; Lenggoro, I. W.; Okuyama, K. *J. Phys. Chem. Solids* **1999**, *60*, 379.
(20) Joffin, N.; Caillier, B.; Dexpert-Ghys, J.; Verelst, M.; Baret, G.; Garcia, A.; Guillot, P.; Galy, J.; Mauricot, R.; Schamm, S. *J. Phys. D: Appl. Phys.* **2005**, *38*, 3261.
(21) Bazzi, R.; Flores-Gonzalez, M. A.; Louis, C.; Lebbou, K.; Dujardin, C.; Brenier, A.; Zhang, W.; Tillement, O.; Bernstein, E.; Perriat, P. *J. Lumin.* **2003**, *102−103*, 445.
(22) Chandra, S.; Deepak, F. L.; Gruber, J. B.; Sardar, D. K. *J. Phys. Chem. C* **2010**, *114*, 874.
(23) Wong, K. L.; Law, G. L.; Murphy, M. B.; Tanner, P. A.; Wong, W. T.; Lam, P. K. S.; Lam, M. H. W. Inorg. Chem. **2008**, *47* (12), 5190.
(24) Mao, Y.; Huang, J. Y.; Ostroumov, R.; Wang, K. L.; Chang, J. P. *J. Phys. Chem. C* **2008**, *112*, 2278.
(25) Mao, Y.; Guo, X.; Tran, T.; Wang, K. L.; Shih, C. K.; Chang, J. P. *J. Appl. Phys.* **2009**, *105*, No. 094329 (4 pp) .
(26) Muresan, L.; Popovici, E. J.; Grecu, R.; Barbu Tudoran, L. *J. Alloys Compd.* **2009**, *471*, 421.
(27) Trojan-Piegza, J.; Zych, E.; Hreniak, D.; Stręk, W.; Kępiński, L. *J. Phys.: Condens. Matter* **2004**, *16*, 6983.
(28) Bretcanu, O.; Spriano, S.; Brovarone Vitale, C.; Verné, E. *J. Mater. Sci.* **2006**, *41*, 8320.
(29) Li, J. G.; Li, X.; Sun, X.; Ishigaki, T. *J. Phys. Chem. C* **2008**, *112*, 11707.
(30) Dulina, N. A.; Yermolayeva, Y. V.; Tolmachev, A. V.; Sergienko, Z. P.; Vovk, O. M.; Vovk, E. A.; Mateevskaya, N. A.; Mateychenko, P. V. *J. Eur. Ceram. Soc.* **2010**, *30*, 1717.
(31) Matijevic, E.; Hsu, W. P. J. Colloid Interface Sci. **1987**, *118* (2), 506.
(32) Aiken, B.; Hsu, W. P.; Matijevic, E. *J. Am. Ceram. Soc.* **1988**, *71* (10), 845.
(33) Matijevic, E. *Chem. Mater.* **1993**, *5*, 412.

2.b. Characterization Techniques. Particle shape and size were examined via TEM, using a Philips Model CM20 FEG microscope.

WAXS analysis was performed on small amounts of powder sealed in Lindemann glass capillaries. Measurements of the X-ray intensity scattered by the samples irradiated with graphite monochromatized Mo Kα (0.071069 nm) radiation were performed using a dedicated two-axis diffractometer. The measurement time was 20 h for each sample. Data were corrected for polarization and absorption effects and empty capillary scattering, then normalized and Fourier-transformed to obtain the radial distribution function (RDF).

Chemical bonding was analyzed by infrared spectroscopy, using a Perkin−Elmer 100 Series spectrometer. Samples were prepared by mixing the powders with potassium bromide (1/100 by weight) in a pellet. Thermogravimetric analysis (TGA) was realized using a SETARAM Model Labsys TG-DTA 16 apparatus, working in an O_2 atmosphere with a heating rate of 10 °C/min.

To investigate small quantities of matter, a "micro-Raman" setup was employed: the Eu^{3+} luminescence was investigated with a Dilor XY (UV) spectrometer equipped with a CCD detector. Excitation was achieved by the line at 488 nm of a Kr−Ar laser. Exciting light was directed through a microscope on the sample crushed on a glass plate. Alternatively, the luminescence of solid samples or colloidal solutions was also studied with a Jobin−Yvon Model Fluorolog FL3-22 spectrometer that was equipped with a R928 Hammamatsu photomultiplier and a 450-W Xe excitation lamp. For the analysis of the emission decay versus time, a pulsed Xe source was employed. The emission decays have been recorded under excitation at 254 nm, monitoring the $^5D_0 \rightarrow {}^7F_2$ at its maximum. The experimental curves were fitted by the single exponential $I(t) = I_0 \exp(-t/\tau)$. The I_0/e lifetimes (defined as τ) were thus calculated, with an error range estimated to be ±15%.

2.c. Cell Culture and Nanoparticle Exposure: Fluorescence Imaging. Human cervical carcinoma (HeLa) cells were maintained in an RMPI 1640 medium supplemented with 10% fetal bovine serum (FBS) and 1% penicillin and streptomycin in 5% CO_2. For nanoparticles exposure, cells that had been diluted within a range of 1:2 to 1:4 were plated onto 60 mm × 15 mm culture dishes at 2 mL per dishes. One sterile 18 mm × 18 mm glass coverslip was placed in each dish before the cells were added. Cells were allowed to attach for 2 days. Stock solutions of 1 mg/mL of NPs were prepared in phosphate buffer solution (PBS) and sonicated at room temperature for 30 min, prior to being added to the cells. Stock solutions were added to the cells in a supplemented medium at a ratio of 1:200. After exposure, the medium was removed and cells were washed two or three times with PBS, and 2 mL of medium was added again. For the in vitro imaging, the cells (HeLa) were imaged in the tissue culture chamber (5% CO_2, 37 °C) using a Leica Model SP5 (upright configuration) confocal microscope equipped with argon laser and a femtosecond-pulsed Ti:sapphire laser (Libra II, Coherent). The excitation beam produced by the argon laser, which was tunable from 457 nm to 514 nm and was focused on coverslip-adherent cells, using a 40× oil-immersion objective.

3. Results

3.a. TEM Imaging of the Particles. Some characteristic images of the solid phases extracted at different maturation times are displayed in Figure 1. Until 240 min (t12), the particles are spherical and well-monodispersed in size. The average diameter is 164 ± 22 nm for t6 and 240 ± 19 nm for t12. At longer times (270 min, sample t13), a few platelet-like particles appear. The platelet particles grow and aggregate themselves with time, whereas the diameter of the spherical particles decreases. Spherical particles tend to disappear to the benefit of much bigger aggregates of platelet-shaped crystals (images t13, t14, t16). These observations are summarized in Table 1.

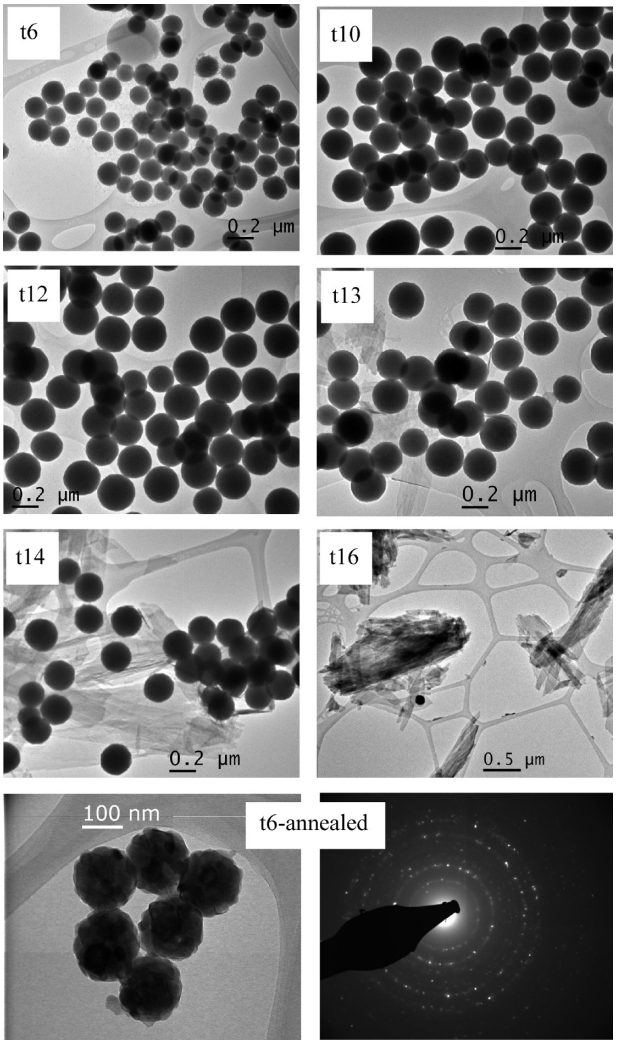

Figure 1. TEM imaging of particles sampled at different maturation times (t1 to t16). Bottom images show a TEM photomicrograph and the electronic diffraction pattern of a t6-annealed sample.

3.b. Characterization of the Solid Obtained after a Maturation Time of 420 Min (t16). The sample obtained for the longest reaction time, at t16, was analyzed by WAXS, TGA, infrared (IR), and luminescence spectroscopy.

On the WAXS diffractogram (Figure 2a), narrow peaks, corresponding to the diffraction by crystals are observed. These peaks may unambiguously be assigned to $Gd_2(CO_3)_3 \cdot (2-3)H_2O$, by comparison with the ICDD data (File Card No. 37-0559), revealing that the platelet-like particles were made of hydrated gadolinium carbonate.

The TGA curve of sample t16, displayed in Figure 3, is in good agreement with the observations detailed in ref 34, which describes the decomposition of $Gd_2(CO_3)_3 \cdot (2-3)H_2O$. The total weight loss measured here between 30 °C and 720 °C is 37%, which is slightly higher than the 34%

(34) Park, I. Y.; Kim, D.; Lee, J.; Lee, S. H.; Kim, K. J. *Mater. Chem. Phys.* **2007**, *106*, 149.

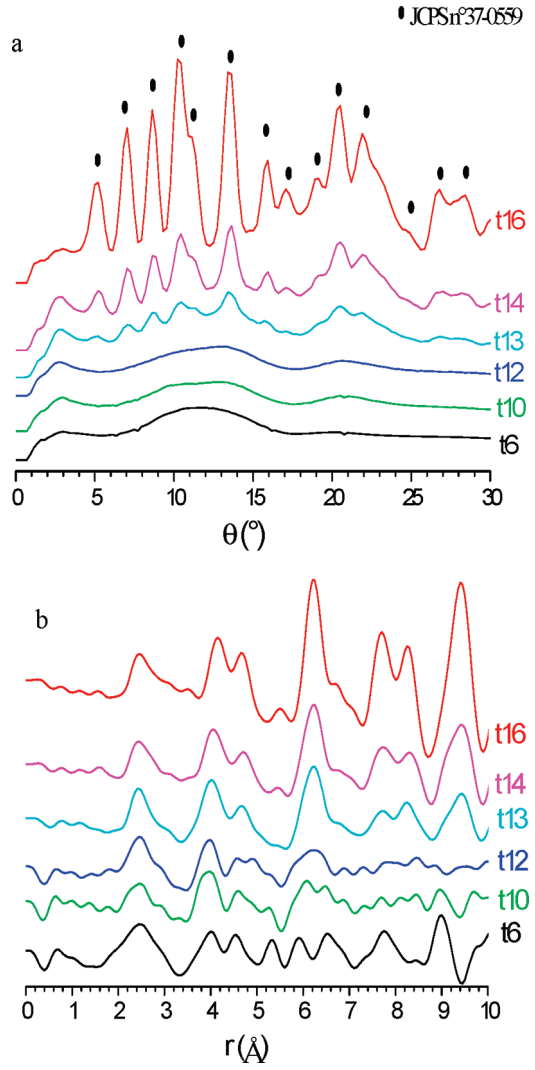

Figure 2. WAXS measurements: (a) corrected diffractograms of particles sampled at different maturation times, and (b) related radial distribution functions (RDFs).

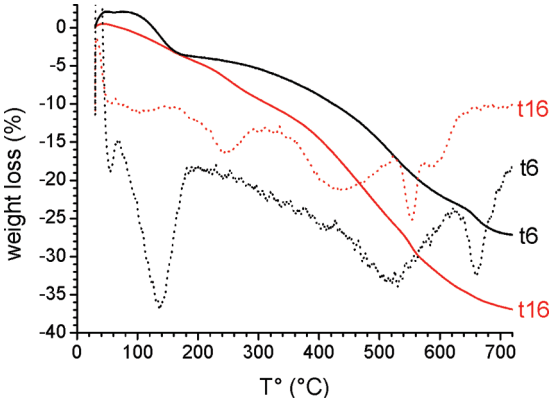

Figure 3. TGA curves (full lines) and DTG curves (dot lines) of samples (a) t6 and (b) t16.

calculated with 3 H_2O in the formulas. The decomposition occurs in four steps, evidenced by peaks in the differential thermogravimetry (DTG) differential curve. The two peaks at 120 and 260 °C are linked to the dehydration of the material: the first one, centered at 120 °C, is due to the removal of adsorbed water, and the second one, at 260 °C, is due to the elimination of structural water. The broad peak at ~440 °C relates to the loss of two carbonate groups per unit formula, to give the oxycarbonate. The narrower peak at 560 °C corresponds to the loss of one carbonate when the oxycarbonate transforms to an oxide. Our observations might be summarized by eq 1:

$$Gd_2(CO_3)_3 \cdot 3H_2O \xrightarrow[-3H_2O]{30\ °C<T<325\ °C} Gd_2(CO_3)_3 \xrightarrow[-2CO_2]{325\ °C<T<530\ °C} Gd_2O_2CO_3 \xrightarrow[-CO_2]{530\ °C<T<700\ °C} Gd_2O_3 \quad (1)$$

The FTIR spectrum of sample t16 (Figure 4) exhibits very narrow and well-defined bands between 650 cm^{-1} and 1550 cm^{-1}, attributed to several vibration modes of the carbonate $(CO_3)^{2-}$ groups. The thinness of these bands is characteristic of a well-crystallized material. The detailed assignment of these bands (with the Herzberg's notation) is gathered in Table 2. Bands corresponding to $\nu(H_2O)$ and $\delta(H_2O)$ are also seen at 3420 and 1646 cm^{-1}, respectively. Our observations are in good agreement with those reported

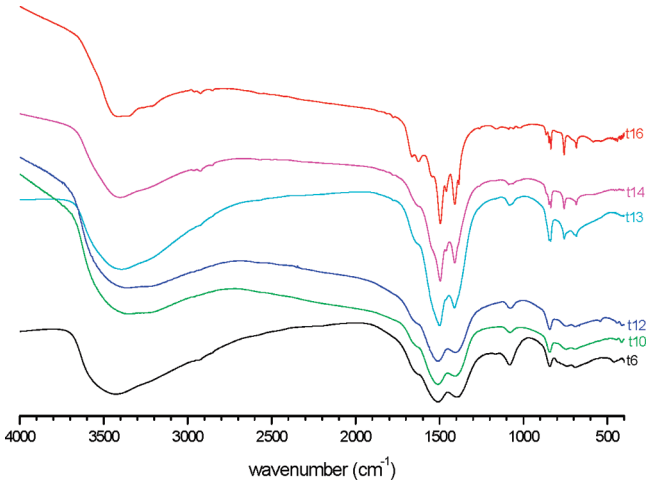

Figure 4. Infrared (IR) spectra of particles sampled at different maturation times.

Table 2. Observed IR Absorption Frequencies and Assignment

	ν_3 (cm^{-1})	ν_1 (cm^{-1})	ν_2 (cm^{-1})	ν_4 (cm^{-1})	δ_{H_2O} (cm^{-1})
t6	1400, 1512	1081	848	650−800	1640
t10	1400, 1512	1081	848	650−800	1640
t12	1400, 1512	1081	848	685, 752	1640
t13	1413, 1501	1081	848	685, 759	1640
t14	1413, 1462, 1494, 1551	1081	837, 847	685, 759	1640
t16	1384, 1410, 1462, 1494, 1551		837, 847, 865	685, 759	1620, 1646

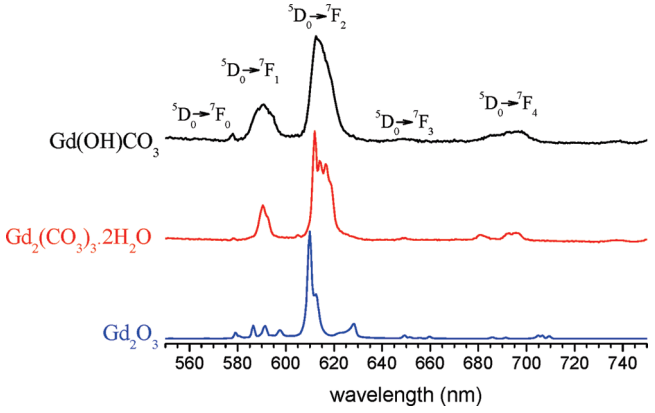

Figure 5. Eu^{3+} emission spectra recorded under excitation at 254 nm for sample t6 ($GdOHCO_3$), t16 ($Gd_2(CO_3)_3 \cdot 2H_2O$) and t6-annealed (Gd_2O_3).

by Park et al.[34] on samples from urea-assisted synthesis and with the former study by Sungur et al.,[35] who slowly crystallized gadolinium carbonate after the hydrolysis of gadolinium trichloroacetate. For our sample t16, we have identified five components for the ν_3 mode, whereas ν_1 is almost silent. The weak differences between our spectrum and those displayed in refs 34 and 35 illustrate the dependency of the infrared (IR) data on the preparation conditions, especially dealing with, more or less, well-crystallized hydrated samples. The observation of three ν_2 and five ν_3 distinct components supports the existence of two carbonate groups, and the presence of two $\delta(H_2O)$ may be assigned to two types of water molecules.

To the best of our knowledge, the structure of the gadolinium hydrated carbonate has not been solved, but numerous previous works have established that $Gd_2(CO_3)_3 \cdot 2H_2O$ crystallizes with the tengerite-type orthorhombic structure, isomorphous to the yttrium hydrated carbonate $Y_2(CO_3)_3 \cdot 2H_2O$. The crystal structure of tengerite-(Y) was redefined by Miyawaki et al.,[36] and the description given by these authors also is pertinent for tengerite-(Gd). It is composed of corrugated sheets of 9-fold-coordinated Y(Gd) polyhedra. One type of carbonate group participates in the coordination polyhedron of the cation within the sheets, whereas the other carbonate links the sheets to form a three-dimensional framework. The two structural water molecules participate in the Y(Gd) coordination. Therefore, the tengerite-type carbonate has a lamellar structure, which matches very well with the platelet morphology observed in our samples at longer maturation times.

The luminescence emission spectrum of Eu^{3+} in the carbonate $(Gd_{0.95}Eu_{0.05})_2(CO_3)_3 \cdot 2H_2O$ (sample t16) (Figure 5) exhibits some characteristic features related to the local crystal field at the metal site. The point symmetry at the metal ion is C_1, so that the maximum number of components could be observed a priori (i.e., $2J + 1$ components for each $^5D_0 \rightarrow {}^7F_J$ Eu^{3+} emission transition). Actually, two, four, one, and three components were separated by deconvoluting the $^5D_0 \rightarrow {}^7F_1$, $^7F_2$, $^7F_3$, and $^7F_4$ transitions, respectively. The corresponding wavelengths are gathered in Table 3. The $^5D_0$ I/e lifetime is 0.67 ± 0.10 ms.

3.c. Characterization of the Solid Obtained between Maturation Times of 120 min (t6) and 300 min (t14). Some characteristic FTIR spectra are displayed in Figure 4. At short maturation times (samples t6, t10), the spectra exhibit bands assigned to the vibration modes of the carbonate groups, as referenced in Table 2. All features are broader than those observed for t16, and the ν_1 mode at 1081 cm^{-1} is clearly visible. The $\delta(H_2O)$ is observed at 1646 cm^{-1}, as well as a very broad $\nu(H_2O)$ band. The FTIR spectra observed for t13 and t14 exhibit the same bands, more and more well-resolved.

The Eu^{3+} photoluminescence of the same samples was analyzed with a micro-Raman setup. Figure 6 displays the emission transitions $^5D_0 \rightarrow {}^7F_0$, $^7F_1$, and $^7F_2$ for some samples. Compared to that of t16, the spectra recorded for t6 to t12 samples are characterized by a relatively more-intense $^5D_0 \rightarrow {}^7F_0$, three overlapping $^5D_0 \rightarrow {}^7F_1$ with $\sim$156 cm^{-1} splitting and a broad $^5D_0 \rightarrow {}^7F_2$. The emission lines are broad, because the local fields that are exerted on each Eu^{3+} ion differ. Such inhomogeneous broadening has been described in many types of amorphous phases or glasses. Samples t13 to t16 were actually mixtures of the amorphous (t6 type) and the crystallized (t16 type) particles: both types of Eu^{3+} emission spectra could be recorded, depending on the grains present in the light/matter interaction volume. The characteristic emission wavelengths observed at t6 are gathered in Table 3. The $^5D_0$ emission lifetime (0.64 ± 0.10 ms) is equal to that measured for t16.

The evolution of the structure of the solid phase is also very well-evidenced by the diffractograms (Figure 2a). Well-defined diffraction lines were observed for sample t16. The diffractograms measured on samples t14 and t13 display most of these lines, although their peak-to-background ratio is greatly reduced. Powders sampled at shorter times exhibit only broad features.

From the first work by Matijevic and Hsu,[31] it has been assumed that the solid phase synthesized in our experimental conditions is a "basic" carbonate. The chemical analysis performed on gadolinium compounds in that pioneering work led to the formula $Gd(OH)CO_3 \cdot H_2O$. The same composition, although with only half a water molecule per Gd atom, was reported in ref 37, where the thermal decomposition of a series of lanthanides and yttrium carbonates was studied. The TGA curve measured on our sample t6 is shown in Figure 3. First, there is a weight uptake and then an abrupt loss at T(< 200 °C); the net loss of 4% is caused by the removal of one hydration water (H_2O) per two Gd atoms. The weight loss between 200 °C and 800 °C (24%) fits well with the elution of one H_2O molecule and two CO_2 molecules for two Gd atoms. The total weight loss between 30 °C and 800 °C is 28% (26% calculated), according to eq 2.

(35) Sungur, A.; Kizilyall, M. *J. Less Common Met.* **1983**, *93*−*2*, 419.
(36) Miyawaki, R.; Kuriyama, J.; Nakai, I. *Am. Mineral.* **1993**, *78*, 425.
(37) Moscardini d'Assuncao, L.; Giolito, I.; Ionashiro, M. *Thermochim. Acta* **1989**, *137*, 319.

Table 3. Characteristics Wavelengths of the Eu^{3+} Emission in Samples at t16, t6, and t6-Annealed

	$^5D_0 \rightarrow {}^7F_0$	$^5D_0 \rightarrow {}^7F_1$	$^5D_0 \rightarrow {}^7F_2$	$^5D_0 \rightarrow {}^7F_3$	$^5D_0 \rightarrow {}^7F_4$
t16 (tengerite-(Gd))	578	590.5, 592.5	605, 612, 614, 616.5	649.5	680.5, 692.5, 695.5
t6 (amorphous)	578	588.5, 591.5, 593.5	612.5	648.5	696
t6-annealed (C-Gd_2O_3)	579	580.6, [a] 586.5, 591.5, 597.5	610, 612.5, 622, 628	649.5, 651.5, 655.5, 659.5, 664.5	685.5, 691.5, 705, 706.5, 709.5

[a] $^5D_0 \rightarrow {}^7F_1$ transition of Eu^{3+} with C_{3i} symmetry.

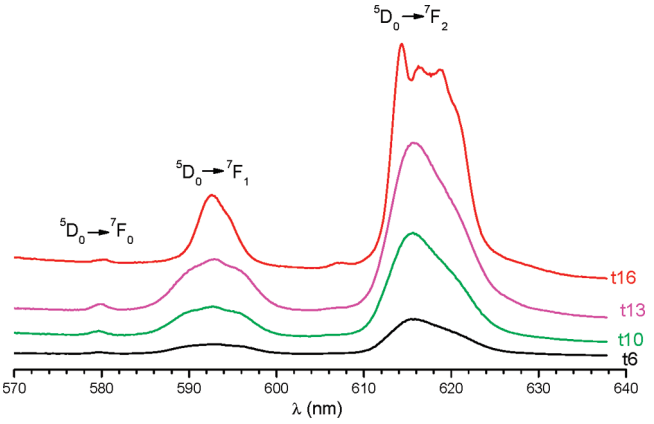

Figure 6. Emission spectra of particles sampled at different maturation times (λ_{ex} = 488 nm). The spectra are displayed without normalization.

There is a sudden event at 660 °C, which corresponds to the decomposition of the dioxy-monocarbonate to the oxide. Therefore, sample t6 is an amorphous hydroxycarbonate, which decomposes via the following mechanism:

$$Gd_2(OH)_2(CO_3)_2 \cdot H_2O \xrightarrow[-H_2O]{20\ ^\circ C<T<200\ ^\circ C} Gd_2(OH)_2(CO_3)_2 \xrightarrow[-H_2O-CO_2]{200\ ^\circ C<T<630\ ^\circ C} Gd_2O_2CO_3 \xrightarrow[-CO_2]{630\ ^\circ C<T<720\ ^\circ C} Gd_2O_3 \quad (2)$$

As described in section 3.a, sample t6 is made of spherical nanoparticles with a uniform size. We have chosen these nanoparticles for further investigations of their PL characteristics in colloidal suspensions or in living cells. In parallel, part of sample t6 has been transformed to an oxide, as described in section 3.d. Then, we have compared the PL characteristics of t6-annealed and t6 recorded under the same conditions.

3.d. Annealing of Sample t6. Following the TGA curve, the transformation of $Gd(OH)CO_3$ to an oxide is achieved at a temperature of 720 °C. A moderately higher temperature (850 °C) was chosen to anneal sample t6 for 4 h under air. After this treatment, the only crystalline phase detected was C−Gd_2O_3, in agreement with the ICDD data (File Card No. 4-0473). Particles do not agglomerate and keep their spherical and uniform size after the heating treatment. The electronic diffraction micrograph that has been recorded from one particle (Figure 1) exhibits well-defined spots, meaning that it consists of several nanocrystals present in the selected area. The nanocrystals size could be estimated from the TEM image contrast (~10−50 nm).

The Eu^{3+} emission spectrum, displayed in Figure 5, has narrow lines, as expected for a well-crystallized powder. The observed emission wavelengths (gathered with their assignment in Table 3) are in full concordance with those reported in the literature for C-Y_2O_3 and C-Gd_2O_3. The lifetime measured for Eu^{3+} in Gd_2O_3 (i.e., $\tau = 1.43 \pm 0.21$ ms) is in reasonable agreement with those reported for commercial phosphors ($(Y_{0.95}Eu_{0.05})_2O_3$) measured under similar conditions: τ = 1.1 ms[5] or, for $(Y_{0.90}Eu_{0.10})_2O_3$ with a crystallite size of 80 nm, τ = 1.39 ms.[38] Here, it is not possible to compare our numerical value with all those reported in the literature. They are dependent on the matrix (Y_2O_3, Gd_2O_3, Lu_2O_3), the Eu doping, the crystals sizes, and the details of the measurements. For comparison, we consider a value of τ = 1.43 ms in the oxide, and we measured under the same experimental conditions.

3.e. Luminescence Properties of the Colloidal Suspensions. As it has been said, the objective of this work was to test the possibility to employ the synthesized nanoparticles for biolabeling. In this scope, we have investigated the PL characteristics after being dispersed in water at 1 mg/mL. Expressed in number of NPs, this value turns out to be 8.1×10^{13} NPs of $Gd(OH)CO_3$ per liter of solution and 5.7×10^{13} NPs of Gd_2O_3 per liter of solution, while the average concentrations of Eu^{3+} ions are 2.1×10^{-4} and 2.8×10^{-4} M, respectively. The stability of the colloidal suspensions against agglomeration has been checked by controlling the optical absorption in the visible range: the decrease of absorbance was <20% over 30 min. The Eu^{3+} emission spectra are given in Figure 7, together with those of the dried powders. The main features noticed for the powders are also well-observed in suspensions. The $^5D_0$ lifetimes are also the same in dried samples and in their colloidal suspensions (0.60 ± 0.09 ms for hydroxycarbonate, 1.37 ± 0.20 ms for the oxide). All these observations prove that NPs are stable against chemical degradation in water.

The integrated emission intensities, measured in the wavelength range of $^5D_0 \rightarrow {}^7F_{0-4}$ transitions, for the colloidal suspensions are gathered in Table 4. Under excitation at 393 nm (in the $^7F_0 \rightarrow {}^5L_6$ transition of Eu^{3+}), the hydroxycarbonate and the oxide emissions have about the same intensities. We will address this important point in the discussion. The relative intensities are drastically different under excitation within the ligand-to-metal

(38) Zhang, W. W.; Xu, M.; Zhang, W. P.; Yi, M.; Qi, Z. M.; Xia, S. D.; Garapon, C. *Chem. Phys. Lett.* **2003**, *376*, 318.

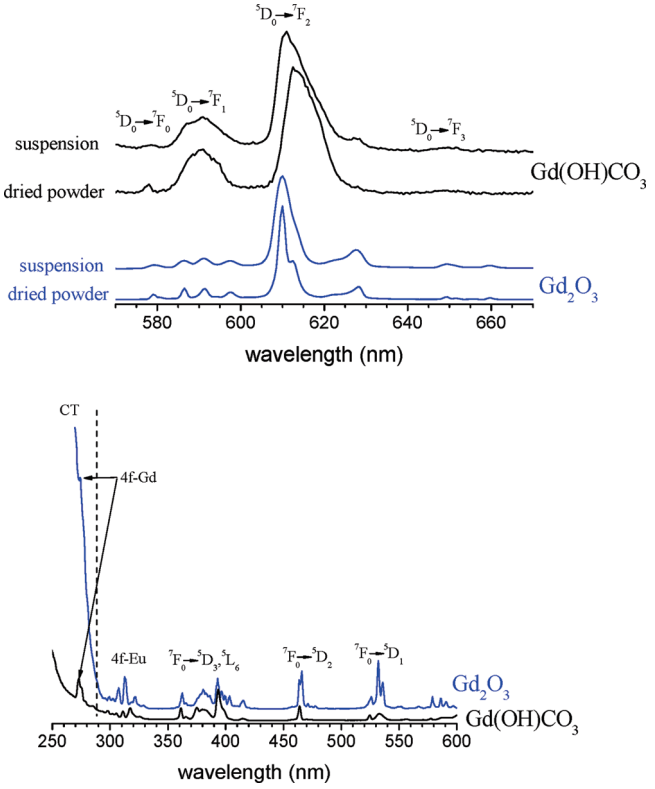

Figure 7. (Top) Eu^{3+} emission spectra under excitation at 254 nm for dried samples t6 ($Gd(OH)CO_3$) and t6-annealed (Gd_2O_3) and for their suspension at 1 mg/mL in water. (Bottom) Excitation spectra monitored at 610 nm.

Table 4. $^5D_0$ Lifetimes and Integrated Intensities Recorded for Powders Dried and in Suspensions

sample		τ (λ_{ex} = 254 nm)	I (λ_{ex} = 254 nm)	I (λ_{ex} = 393 nm)
t6	solid	0.64 ms		
$Gd(OH)CO_3:Eu^{3+}$	suspension	0.60 ms	3	7
t6-annealed	solid	1.43 ms		
$Gd_2O_3:Eu^{3+}$	suspension	1.37 ms	100	5
t16	solid	0.67 ms		
$Gd_2(CO_3)_3 \cdot 2H_2O:Eu^{3+}$	suspension	0.59 ms	2	5

charge-transfer (CT) state at 254 nm: in that case, the emission by the hydroxycarbonate is just 3% of that of the oxide. This is well-supported by the comparison of the corresponding excitation spectra (see Figure 7). We observe that absorption at 254 nm is remarkably insufficient to excite the Eu^{3+} emission in the hydroxycarbonate, contrary to what happens in the oxide host, where a very strong excitation band is seen at wavelengths < 280 nm.

3.f. Observation of Particles Fluorescence in Living Cells. The spherical particles (hydroxycarbonate or oxide) doped with Eu^{3+} have been allowed to react under controlled conditions, as described in the Experimental Section, with HeLa cells. The confocal fluorescence microscopy images displayed in the left side of Figure 8 were obtained under an excitation wavelength of 514.5 nm and filtered in the emission range of 550−670 nm. The Eu^{3+} luminescence can be seen as well under excitation at 488 nm. Both wavelengths are located between $^7F_0 \rightarrow {}^5D_1$ and $^7F_0 \rightarrow {}^5D_2$ and are

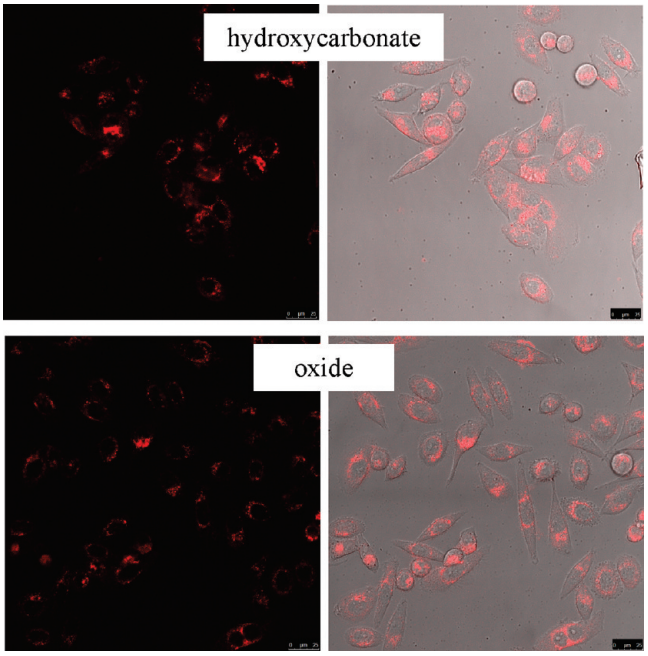

Figure 8. Confocal fluorescence microscope images of human cervical carcinoma (HeLa) cells after 12 h of exposure to europium-doped gadolinium ((top) hydroxycarbonate and (bottom) oxide).

able to excite the Eu^{3+} ions in the $^5D_1$ level. The right side of Figure 8 shows these fluorescence images superimposed on bright-field images of the same zone. It appears that nanoparticles have been internalized by the cells, since a red fluorescence is observed in the cytoplasm, and it is more intense around the nucleus. Similar observations were made for the hydroxycarbonate and the oxide NPs, which appeared to be internalized in similar ways by the cells.

4. Discussion

The discussion coming out these results will be decomposed in two parts: The first part deals with structural aspects: the results of the investigation step by step of the precipitation will be compared with previously published works. The second part deals with the PL characteristics of selected particles in colloidal suspensions or in cells.

4.1. Structural Aspects. The crystallized phase that appears at the end of the urea-assisted precipitation (sample t16, extracted after 7 h) has been very well-identified by X-ray diffraction, using the WAXS conditions, as required for these weakly scattering samples. It is assigned to be the so-called tengerite $Gd_2(CO_3)_3 \cdot 2H_2O$. The thermal analysis and the FTIR spectra are in very good agreement with this formulation. To probe the chemical and structural changes in the solids by interpreting the Eu^{3+} luminescence, europium has been introduced in partial substitution for gadolinium (95Gd/5Eu). The emission spectrum recorded at t16 is thus assigned to Eu^{3+} in tengerite-(Gd), which has not been reported elsewhere. In ref 34, the authors have performed a systematic investigation of the crystalline phases obtained with the urea-assisted method at various temperatures (T_{syn}), using concentrated solutions of [Gd + Eu] = 0.05 M and [urea] = 0.5−2.5 M (versus 0.005 M and 0.5 M, respectively, in our case). Three hours after

the beginning of the precipitation, the powders were identified as tengerite with a platelet shape when $T_{syn} = 80$ °C, and as $Gd_2O(CO_3)_2 \cdot H_2O$ when the temperature increases to T_{syn} = 100 °C. Tengerite-(Y) particles have also been obtained under hydrothermal conditions by Zhang et al.[39] In their work, concentrated solutions ([Y] = 0.05 M and [urea] = 0.05−0.15 M) were heated in an autoclave at 150 °C for 22 h. Rodlike $Y_2(CO_3)_3 \cdot 2H_2O$ powders were obtained when the [Y]:[urea] ratio was 1:3, changing to dumbbell-like $YOHCO_3$ at a 1:1 ratio. In the present work, we put forward some different observations, since no trace of the crystallized $Gd(OH)CO_3$ or oxo-carbonates have been identified. These differences may arise from the experimental conditions employed, since we performed the precipitation from diluted solutions at moderate temperature.

Our synthesis conditions were chosen according to the paper by Matijevic et al.,[31] where nanoparticles with a composition of $Gd(OH)CO_3 \cdot H_2O$ had been obtained. Actually, we reached almost the same formulation for our sample extracted after 2 h (sample t6). For t6, the total weight loss during decomposition fits well with $Gd(OH)CO_3 \cdot 0.5H_2O$. The FTIR spectrum exhibits the C−O and O−H vibration modes. However, there is no evidence of isolated hydroxyl groups as has been observed in crystallized dehydrated $Nd(OH)CO_3$,[40] since the broad band observed in the 3400−3600 cm^{-1} range comes from all hydroxyls, including water molecules. The solid phase is made only of spherical nanoparticles (diameter = 164 ± 22 nm), which can be considered to be amorphous. However, the first peaks on the related RDF suggest a large distribution of Gd−O bonding distances centered on 0.245 nm and a better-defined Gd−Gd distance at 0.40 nm, in agreement with the short-range order present in the $Gd(OH)CO_3$ structure.[41] Additional information is given by the Eu^{3+} optical probe. The emission displays structureless features that are characteristic of Eu^{3+} ions in an amorphous matrix. The $^5D_0$ emitting-level lifetime is an indicator of the vibration modes of the species in the Eu^{3+} first coordination shell. In the carbonate (t16), europium that is substituting for gadolinium is coordinated by 9 oxygens, 8 of them from carbonate groups (3 bidentate and 2 monodentate) and one from water molecule (i.e., two O−H vibrators).[36] The $^5D_0$ lifetime is 0.67 ± 0.09 ms. On the other hand, the emission lifetimes of several europium carbonate complexes in water have been determined by Plancque et al.[42] They measured lifetimes of 0.44 ± 0.04 ms for the tris-carbonate complex $Eu(CO_3)_3^{3-} \cdot 2H_2O$, when the rare earth is coordinated by six oxygens from three bidentate carbonates and two oxygens from two water molecules (four O−H vibrators). The $^5D_0$ lifetime that we measured for the t6 sample is very close to that measured for t16 and is significantly higher than that reported for the europium tris-carbonate complex. Our conclusion is that Eu^{3+} ions of t6 particles are also coordinated by six oxygens from three bidentate carbonates and by two or three hydroxyl groups. We have thus shown, as it is schematized in eq 3, that there is a reaction between the hydrated hydroxycarbonate and additional $(CO_3)^{2-}$ groups coming from the continuous decomposition of urea, to give the hydrated carbonate: this had not been reported previously.

$$Gd_2(OH)_2(CO_3)_2 \cdot H_2O + CO_3^{2-} + 2H^+ \rightarrow Gd_2(CO_3)_3 \cdot 2H_2O + H_2O \quad (3)$$

The reaction may be followed step by step, considering each of the characterization techniques employed, as it has been detailed here above in section 3.c. The main point to keep in mind is that few platelets have been first imaged in sample t13, growing as the spheres tended to disappear at longer maturation times. At the same time, more-structured diffraction peaks are observed, unambiguously, because of the apparition of $Gd_2(CO_3)_3 \cdot 2H_2O$, and linked with the disappearance of the spheres, from t14 to t16. We thus conclude that the synthesis must be stopped before the appearance of $Gd_2(CO_3) \cdot 2H_2O \cdot Eu^{3+}$ crystals. Doing so, only $Gd(OH)CO_3$:Eu^{3+} nanoparticles that are spherical, monodispersed in size, and amorphous are recovered. These nanoparticles may then be transformed to the oxide C-Gd_2O_3:Eu^{3+} by thermal annealing. Oxide NPs are spherical, with no interparticulate agglomeration.

4.2. Photoluminescence. The photoluminescence of the two types of nanoparticles ($Gd(OH)CO_3$:Eu^{3+} and Gd_2O_3:Eu^{3+}) has been investigated after their dispersion in water at the same level: 1 mg/mL. These measurements have been performed first, to control the chemical stability of the particles. Since the shape of the emission spectrum and the $^5D_0$ lifetime were the same before and after dispersion, one can safely conclude that the NPs have not been modified.

On the other hand, we assume that the integrated PL intensities emitted by the suspensions may be compared, provided that the measurements are performed with same instrumental conditions. We have noticed that, when excitation is achieved in one of the $Eu^{3+}(4f^6)$ electronic levels (i.e., $^5L_6$), then the PL characteristics of the hydroxycarbonate and that of the oxide suspensions have the same intensities. For the observations of the europium-doped NPs in living cells, excitation was achieved by the 514-nm or 488-nm argon laser lines. Both wavelengths promote the Eu^{3+} ions into a $4f^6$ excited state (here, $^5D_1$), and, under the same observation conditions, the PL recorded for the hydroxycarbonate and for the oxide will be similar. In agreement with these findings, we have observed that the red emissive stainings produced by both types of NPs in cells have the same strength.

In ref 23, some of us have investigated the internalization by human lung carcinoma A549 and by human cervical carcinoma HeLa cells of unfunctionalized europium hydroxide nanorods, and of the same particles coated with an organically modified silicate layer. Patra et al.[43] reported on

(39) Zhang, Y.; Gao, M.; Han, K.; Fang, Z.; Yin, X.; Xu, Z. *J. Alloys Compd.* **2009**, *474*, 598.
(40) Dexpert, H.; Caro, P. Mater. Res. Bull., **1974**, *9* (11), 1577.
(41) Tahara, T.; Nakai, I.; Miyawaki, R.; Matsubara, S. *Z. Kristallogr.* **2007**, *222*, 326.
(42) Plancque, G.; Moulin, V.; Toulho, P.; Moulin, C. *Anal. Chim. Acta* **2003**, *478*, 11.
(43) Patra, C. R.; Bhattacharya, R.; Patra, S.; Basu, S.; Mukherjee, P.; Mukhopadhyay, D. J. Nanobiotechnol. **2006**, *4*, Paper No. 11 (15 pp).

the application of luminescent lanthanide phosphate $EuPO_4$ nanorods in live cell imaging (human umbilical vein endothelial cells (HUVECs) and renal carcinoma cells (RCCs)). In these papers, the inorganic nanoparticles were rodlike, ~20 nm × 500 nm in size. Nanoparticles were readily internalized by cells and exhibited no apparent detrimental effect on cell viability. We have tested the internalization of $Gd(OH)CO_3:Eu^{3+}$ and $Gd_2O_3:Eu^{3+}$ NPs by HeLa cells. A red emission has been observed in the cytoplasm, more intense close to the nucleus; however, no luminescence was detected inside it. Since similar observations had been reported for the hydroxide and for the phosphate nanorods, we suggest that this may reflect a general trend of behavior of living cells toward inorganic nanoparticles.

5. Conclusion

In summary, we have reported the dynamical study of the urea-assisted precipitation of $Gd(OH)CO_3:Eu^{3+}$ luminescent nanoparticles. The chemical and structural changes occurring in the precipitate during the synthesis have been analyzed in detail. The precipitation must be stopped before the appearance of $Gd_2(CO_3)_3 \cdot 2H_2O:Eu^{3+}$ crystals in the medium, to obtain $Gd(OH)CO_3:Eu^{3+}$ spherical nanoparticles (NPs) that have an average diameter of ~160 nm and are amorphous. They may be transformed to crystallized $Gd_2O_3:Eu^{3+}$ nanoparticles, with the same spherical shape and uniform size. The luminescence properties of $Gd(OH)CO_3:Eu^{3+}$ and $Gd_2O_3:Eu^{3+}$ NPs have been investigated and compared in their dried state and after their dispersion as a colloidal suspension. Despite their hydrated and amorphous structure, the hydroxycarbonate NPs have the same luminescence intensity as the oxide NPs under chosen excitation conditions, which is compatible with their observation in living cells. Finally, we have performed some tests of fluorescence imaging in human cervical carcinoma (HeLa) cells, proving that both types of NPs are internalized. Because of their more important reactivity for surface modification, the spherical monodispersed hydroxycarbonate NPs could be considered as better potential luminescent biolabels than the corresponding oxide nanoparticles.

Acknowledgment. The authors thank A. Zwick, S. Joulié, and D. Neumeyer (CEMES-CNRS) for their help in handling the luminescence (Micro-Raman), TEM images, and TGA−DTA experiments. Travel expenses were supported by the Hong Kong−France Research Grant (No. 9050206) of the PROCORE program.